Synchronous and Asynchronous SMB Processes for Gas Separation

José P. B. Mota, Isabel A. A. C. Esteves, and Mário F. J. Eusébio
Requimte/CQFB, Departamento de Química, Faculdade de Ciências e Tecnologia, Universidade Nova de Lisboa, 2829-516 Caparica, Portugal

DOI 10.1002/aic.11162
Published online March 28, 2007 in Wiley InterScience (www.interscience.wiley.com).

The simulated-moving bed (SMB) is now a well established adsorption process for obtaining high-purity products at a similarly high-recovery. In principle the SMB process can be applied to gases, and has been, but application has been limited. Here, we re-examine the SMB process for separation of gaseous components in the light of recent developments in novel cyclic operating schemes and advanced optimization tools. A novel single-column experimental setup is employed to demonstrate the feasibility of the process, explore the effect of its major operating parameters, and illustrate the performance enhancements that are obtained by using an advanced cyclic operation scheme, such as the asynchronous shifting of the inlet/outlet ports. The experimental feasibility and effectiveness of gas-phase SMB are assessed by running and comparing optimized configurations for the separation of CH_4/CO_2 over activated carbon using nitrogen as carrier gas. For this separation, the asynchronous configuration always outperforms the classical SMB scheme, both in productivity and eluent consumption, except at very low-feed throughput where both schemes are coincident. At higher-feed flow rates, the asynchronous scheme quickly diverges from a four-zone, closed-loop configuration towards a three-zone, open-loop process with a 50.6% increase in feed throughput, and 10% reduction on eluent gas consumption. *AIChE J,* 53: 1192–1203, 2007
Keywords: simulated-moving bed, gas separation, varicol process, single-column analog, process design, optimization

Introduction

Simulated-moving bed (SMB) is a continuous adsorptive separation process with numerous applications, many of which are difficult or even impossible to handle using other separation techniques. The SMB process was originally devised as a practical implementation of the true moving bed (TMB) process, where the adsorbent and the fluid phase move countercurrently.[1–3] A mixed feed containing two components, denoted A and B, may be separated by classical SMB into two products: an extract product containing mainly A (the more strongly adsorbed species, or group of species with similarly strong adsorption properties), and a raffinate containing mainly B (the less strongly adsorbed species or group of species).

SMB processes have not generally been used for gas separation,[4] even though it is apparent that under gaseous conditions they combine the high-mass-transfer efficiency of simulated countercurrent operation with the reduced nonselective holdup of the vapor phase. Indeed, in the last few years the feasibility of vapor-phase SMB operation has been demonstrated at laboratory scale for the separation of xylene isomers,[5] linear/nonlinear paraffins,[6] and volatile inhalation anesthetic enantiomers.[7–10] It has been reported[5,6] that units with a small number of columns achieve high-purity performances for some of these separations, provided that the column size and operating conditions are properly designed. SMB processes for other gaseous

Correspondence concerning this article should be addressed to J. P. B. Mota at pmota@dq.fct.unl.pt.

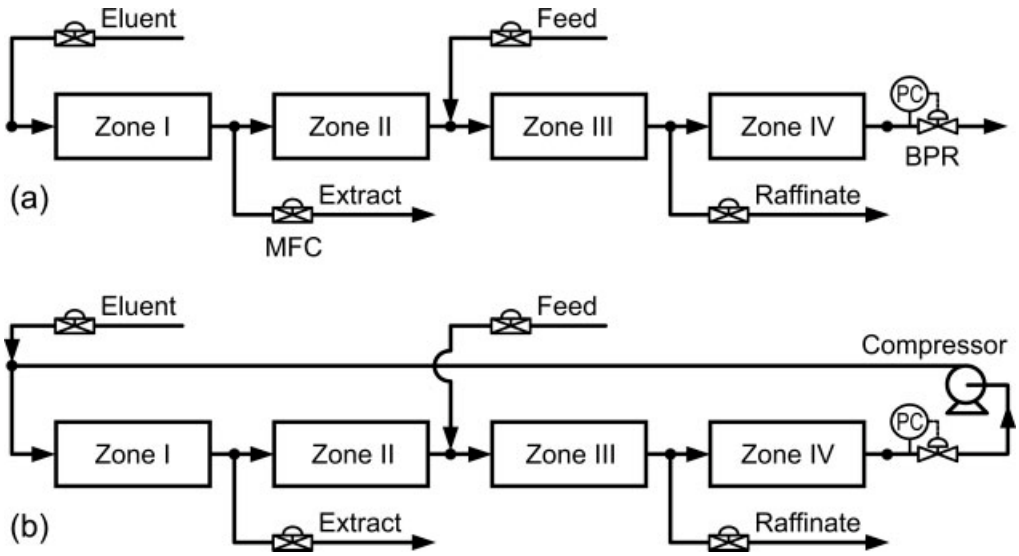

Figure 1. Four-zone (a) open-loop, and (b) closed-loop SMBs for gas-phase operation.

Every switching interval the inlet/outlet ports are moved one column ahead in the direction of gas flow. For simplicity, only the major equipment, such as mass flow controllers (MFC), back-pressure regulators (BPR) and compressor, are drawn.

separations, such as oxygen/argon,[11] production of nitrogen from air,[11] hydrogen/helium,[12] deuterium/helium,[12] and propylene/propane,[13] have been recently disclosed in the patent literature. Even when the adsorbent has a high-selectivity for the adsorption of one component over the other and a good working capacity, it is generally a difficult problem to obtain high-purity products at a similarly high-recovery using an adsorption separation process. SMB processes appear particularly promising for separations where these requirements are mandatory.

Figure 1 shows simplified flow diagrams of four-zone, open- and closed-loop SMBs for gas-phase operation, in which much of the hardware and instrumentation have been deleted as being nonessential to an understanding of the process. The conventional SMB comprises several identical columns, which are serially connected in either a closed or opened-loop configuration. The column sequence is divided into four zones of constant flow rates by four ports: one for adding the gaseous desorbent or carrier gas, another one for withdrawing the slow migrating adsorbates, another one for continuous feeding, and the last one for withdrawing the fast migrating adsorbates. To simulate the movement of a solid bed in opposite direction to the gaseous fluid, the positions of the input and output streams are shifted downstream by one column, at fixed intervals, in the direction of gas flow. Each advancement of the fluid directing device to a new position is generally called a step, and the completion of all valve steps is called a cycle. Details of arranging commercially available two-position and multiposition valves for the operation of the SMB process have been thoroughly reviewed in a recent publication.[14]

Desorption or regeneration take place in zone I and may involve elution,[9] near-isothermal displacement,[6] thermal swing operation in which the desorption zone runs at elevated temperature,[3] or pressure/vacuum swing.[11,13] In Figure 1b, the stream leaving zone IV is recycled back to zone I. This reduces the eluent requirement, but at the cost of installing a compressor in the loop. The flow rates of the eluent and feed inlet streams, as well as those of the extract and raffinate outlet streams, are most conveniently controlled by mass flows controllers. In addition to flow rates, it is necessary to control the pressure level in the unit. In the simplest configuration, the pressure at the outlet of the last column of section IV is fixed by means of a back-pressure regulator. The SMB process is intrinsically dynamic in nature and, as other cyclic adsorption processes, approaches a cyclic steady state (CSS) after a sufficiently long period of operation.

The recent rapid development of SMB applications has led to the introduction of novel SMB schemes[15–23] that are substantially different from the conventional SMB process. The new schemes provide further gains, but usually at the expense of additional complexity. This additional complexity requires highly versatile SMB equipment,[14] advanced optimization tools,[24–30] and robust control procedures.[31–35]

This is the first of a series of articles where we explore the SMB process for gas separation in the light of the recent developments in novel cyclic operating schemes and advanced tools for process optimization. Here, we consider the simplest case, that of the binary separation of an isothermal trace system, that is, an isothermal system where the two adsorbable components are only present at low-concentration in an inert or weakly interacting carrier.

We start by describing the setup which was developed to experimentally explore the SMB process for adsorptive separation from the gas phase. Its practical implementation and operation are described in detail. The discussion is supported by experiments carried out for the separation of CH_4/CO_2 mixture using activated carbon as adsorbent. Nitrogen is used as mobile phase, acting as diluting carrier gas for the feed stream and as eluent. We adopt a recently developed[28] compact representation of synchronous and asynchronous SMB processes as a convenient framework for defining cycle policies and optimizing operating conditions. In particular we examine Varicol[15,16]

operating schemes, where the inlet/outlet ports are shifted asynchronously. By resorting to advanced optimization tools, it is shown that these schemes achieve better performances than the classical SMB in all cases analyzed. The feasibility and effectiveness of these schemes are assessed experimentally.

Experimental Setup

The experimental setup employed in this work is similar to the single-column apparatus recently developed by our group[36] for mimicking the steady periodic behavior of liquid-phase SMBs, but adapted for gas-phase applications. It is worth pointing out that the setup does not actually perform a separation, such as the one proposed in,[37] but is instead employed as a convenient and inexpensive means to establish experimental data that otherwise could only be obtained from a real (expensive) SMB plant. It is obvious that the apparatus can only reproduce multicolumn behavior to a certain extent, because not every practical consideration can be taken into account. For example, it does not reproduce multipacking variability or poisoning and decay of adsorbent capacity. However, it is also true that, in practice, many of these uncertainties are minimized as much as possible when operating a real SMB unit. As we shall demonstrate later, the setup accurately reproduces the intrinsic SMB dynamics, that is, when it is devoided of secondary effects, and increases the confidence in our simulation results. Furthermore, the setup also has other advantages besides the simplicity and compactness that are obtained from the operation of a single column. For example, it is shown below that by correctly selecting the step of the cycle for process startup, the cyclic steady state of the SMB process can be reproduced in a very short experimental run (1–3 cycles) with minimal consumptions of gaseous eluent and adsorbates.

The single-column apparatus is based on the following transformation of the adsorbate material balance applied to the node between any two consecutive columns, say columns $j-1$ and j

$$y_{ij}^{\text{in}}(t) = \begin{cases} \dfrac{Q_{\text{II}}\, y_{ij}^{\text{out}}(t') + (Q_{\text{III}} - Q_{\text{II}})\, y_i^{\text{F}}}{Q_{\text{III}}} & \text{feed port opened} \\ Q_{\text{IV}}\, y_{ij}^{\text{out}}(t')/Q_{\text{I}} & \text{eluent port opened} \\ y_{ij}^{\text{out}}(t') & \text{otherwise} \end{cases} \tag{1}$$

where $t' = t - (N-1)\,\tau$ is a time-delay coordinate, τ is the switching interval, $Q_{\text{I}}, \ldots, Q_{\text{IV}}$ are the internal molar flow rates in the four sections of the SMB, y_i^{F} is the mole fraction of adsorbate i in the feed stream, and the scripts "in" and "out" denote the inlet and outlet of column j, respectively. Clauses "feed port opened" and "eluent port opened" apply to the intervals of the cycle during which column j is in the leftmost position of zone I and zone III, respectively.

Notice that Eq. 1 references solely column j, and that it is identical to the original node balance, except that $y_{i,j-1}^{\text{out}}(t)$ was replaced by $y_{ij}^{\text{out}}(t')$. This substitution is legitimate, because it does not change the steady periodic solution.[37,38]

Provided that $y_{ij}^{\text{out}}(t)$ is known or continuously measured during an experiment, one can feed a single column with a gaseous stream with composition $y_{ij}^{\text{in}}(t)$, defined by Eq. 1, and flow rate $Q(t)$, to mimic the effect of the upstream column. This can be accomplished by using flow control devices, typically mass-flow controllers (MFCs), to continuously adjust three distinct flow rates, Q_i^{in}, according to

$$\begin{cases} Q_1^{\text{in}}(t) = y_1^{\text{in}}(t)\, Q(t) \\ Q_2^{\text{in}}(t) = y_2^{\text{in}}(t)\, Q(t) \\ Q_3^{\text{in}}(t) = Q(t) - Q_1^{\text{in}}(t) - Q_2^{\text{in}}(t) \end{cases} \tag{2}$$

where Q_1^{in} and Q_2^{in} are molar flow rates of pure adsorbate, and Q_3^{in} is the molar flow rate of carrier gas. The admixture of the outlets of the three MFCs replicates the flow rate and composition profile of the internal effluent into the column under the same conditions as those experienced by that column in the SMB unit operating under CSS conditions. As discussed in,[36] $y_i^{\text{out}}(t)$ should preferably be monitored online during the experiment, that is, $y_i^{\text{out}}(t) = \{y_i^{\text{out}}(t)\}^{\text{exp}}$, but it can also be replaced by the steady periodic solution for a suitable process model, $y_i^{\text{out}}(t) = \{y_i^{\text{out}}(t)\}^{\text{sim}}$. In the latter case the experimental outlet composition profile is never fed back into the column, and one is in fact feeding the experimental system with an upstream effluent obtained from a simulated column, that is, $y_i^{\text{in}}(t) = \{y_i^{\text{in}}(t)\}^{\text{sim}}$.

The composition profiles of the extract (y_i^{X}) and raffinate (y_i^{R}) streams are determined from the measured outlet effluent composition, on a mole fraction basis, as follows

$$y_i^{\text{X}} = \frac{Q\{y_i^{\text{out}}\}^{\text{exp}}}{Q_{\text{I}}}, \quad y_i^{\text{R}} = \frac{Q\{y_i^{\text{out}}\}^{\text{exp}} + (Q_{\text{III}} - Q)y_i^{\text{F}}}{Q_{\text{III}}} \tag{3}$$

These expressions apply to the portions of the cycle over which the corresponding withdrawal ports are opened, and take into account the possibility of temporary or full suppression of zone I or zone III.

The one-column apparatus used in this work is illustrated in Figure 2. The adsorbent is packed into a stainless steel (SS) column (3.2 cm ID, 0.9 cm wall thickness) to an adjustable bed length between 40 cm and 60 cm. In order to properly distribute the inlet flow and retain fines, both ends of the column are filled with a small random packing of 5 mm SS solid spheres (3–4 cm bed height), confined between two perforated SS plates, and a thin cotton film as filter. The column is sealed with teflon rings.

Three Pt100 jacketed temperature probes are inserted into the packed bed through high-pressure seals distributed axially along the column. In the experiments reported here, these sensors were merely used to confirm that the process was indeed operating isothermally. Three Pt100 temperature probes are attached to the outer column wall which, together with ancillary tubing (1/8″ ID), are rapped with electric-shielded heating cables to maintain the system at the desired working temperature. The heat dissipated by the cables is adjusted by a digital controller, based on the readings of the Pt100 probes. This temperature control system is effective, but requires operating temperatures at least 5°C above ambient.

A Bronkhorst (USA) back-pressure regulator (BPR), model P-702C-FAC-20R, is placed at the column outlet to maintain the bed pressure at the desired value. This instrument controls pressure in the range 3–16 bar with a 0.5% FS accuracy, and has the added advantage of simultaneously reporting pressure measurements with the same accuracy. The inlet pressure is

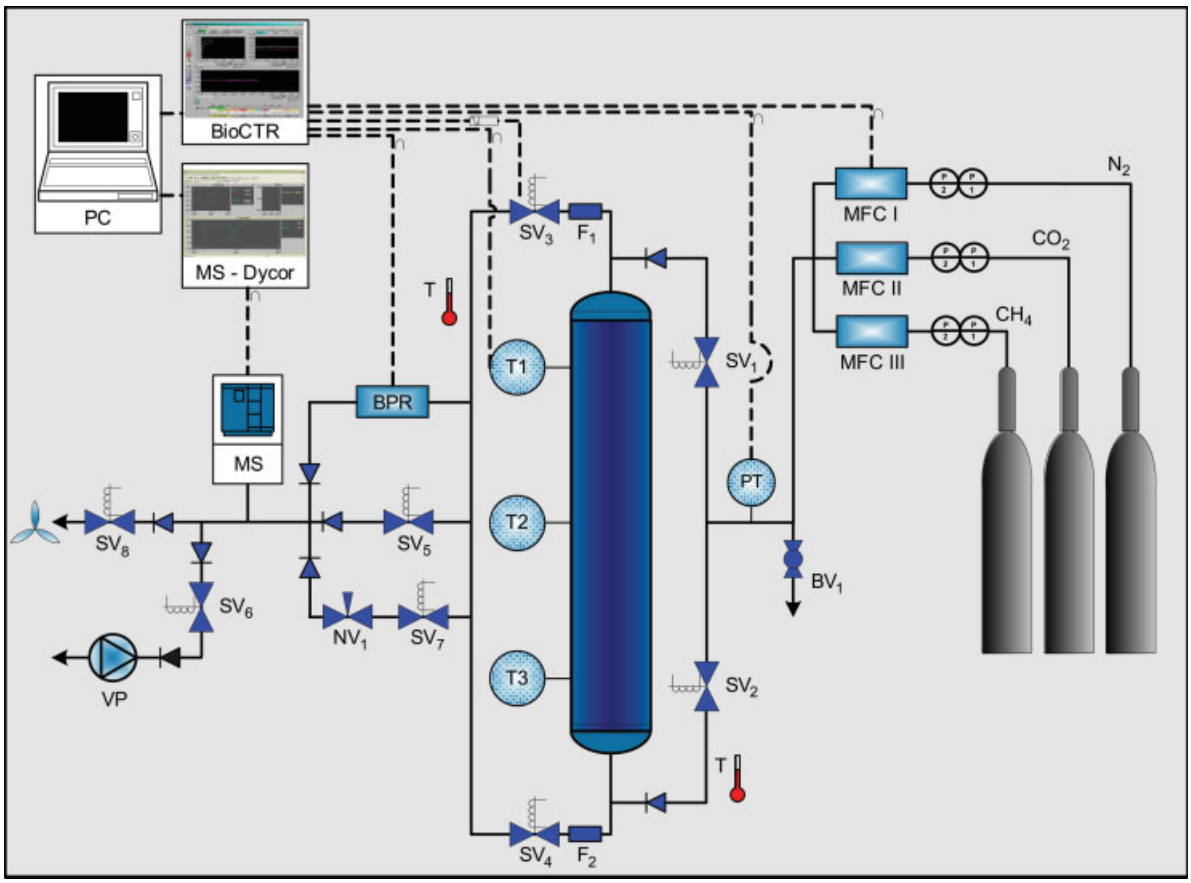

Figure 2. Experimental setup.

Symbols are defined as follows: BPR, back-pressure regulator; MFC, mass-flow controller; SV, solenoid valve; F, filter; BV, ball valve; VP, vacuum pump; MS, mass spectometer. Currently, both BioCTR and Dycor software packages run concurrently on the same computer, but do not communicate with each other. [Color figure can be viewed in the online issue, which is available at www.interscience.wiley.com.]

monitored with a Schaevitz (U.K.) P9071-0003 pressure transducer (0–35 bar, 0.04% FS). All valves are electrically-actuated solenoid type (model Voucomatic, ASCO). Three Teledyne (USA) HFC-202 mass-flow controllers are connected to the column inlet in order to control the composition and flow rate of the inlet effluent. These MFCs provide controlled mass-flow rates in the range 0–0.1 slpm (N_2) for the two adsorbates, and 0–5 slpm (N_2) for the carrier gas, with an accuracy of 1% FS, while simultaneously reporting the measured mass flow rate. The composition of the outlet gaseous effluent is measured by mass spectrometry (MS) using a Dymaxion DM100 quadrupole mass spectrometer from Ametek Process Instruments (USA), operated with Dycor System 2000 software.

The whole setup is fully automated and driven by our Labview-based software system (BioCTR) for process monitoring and control.[39] The Dycor software and BioCTR run concurrently on the same computer, but are not yet able to transfer data between each other. This is due to the lack of the necessary software interface for interprocess communication, which is currently under development by our group. Given the impossibility of feeding back the MS signal into the BioCTR software, $y_i^{\text{out}}(t)$ was replaced by the steady periodic solution of our process model. This is expected to be overcome in the near future.

Column Model

For an isothermal trace system, that is, an isothermal system, where the two adsorbable components are only present at low-concentration in an inert or weakly interacting carrier, changes in fluid velocity across the mass-transfer zone are negligible. For completeness, gas compressibility and pressure drop are taken into account in our formulation.

If the flow pattern can be represented as axially dispersed flow, the differential material balance for the ith adsorbate and overall material balance can be written as

$$\frac{\partial c_i}{\partial t} + \phi \frac{\partial q_i}{\partial t} = \frac{\partial}{\partial z}\left(D_{iL} c \frac{\partial y_i}{\partial z}\right) - \frac{\partial (v c_i)}{\partial z} \tag{4}$$

$$\frac{\mathrm{d}(vc)}{\mathrm{d}z} = 0, \tag{5}$$

where t is time, z is the axial coordinate along the column, c_i is the adsorbate concentration in the gas phase, q_i is the corresponding concentration in the adsorbed phase, y_i is the mole fraction of adsorbate in the gas phase, that is, $c_i = y_i c$, c is the total concentration of the interparticle gas, $\phi = (1 - \varepsilon)/\varepsilon$ is the phase ratio, v is the interstitial gas velocity, and D_{iL} is the dispersion coefficient.

It is further assumed that mass transfer can be approximated by a linear-driving-force (LDF) model. The lumped solid-diffusion version of the LDF model can be written as

$$\frac{\partial q_i}{\partial t} = k_i(q_i^* - q_i) \tag{6}$$

where q_i^* (c_1, c_2) is the adsorption isotherm for solute i, and k_i is the LDF coefficient.

Under linear isotherm conditions, that is, $q_i^* = K_i c_i$, where K_i is the Henry constant for component i evaluated at system temperature T, the model can be replaced by an equilibrium dispersed plug-flow model.[40]

$$(1 + \phi K_i)\frac{\partial c_i}{\partial t} = \frac{\partial}{\partial z}\left(\frac{H_i v}{2} c \frac{\partial y_i}{\partial z}\right) - \frac{\partial (v c_i)}{\partial z} \tag{7}$$

where

$$h_i = \frac{H_i}{L} = \frac{2}{\mathrm{Pe}_i'} = \frac{2}{\mathrm{Pe}_i} + \frac{\phi K_i}{(1 + \phi K_i)^2}\frac{2v}{k_i L} \tag{8}$$

and $\mathrm{Pe}_i' = vL/D_{iL}$ are the dimensionless plate height and apparent Péclet number for the packed column, respectively; L is the column length. It should be pointed out that K_i represents the true Henry constant only if the carrier gas does not interact with the adsorbent. In the case of a weakly interacting carrier gas K_i is the slope of the apparent linear isotherm for a given concentration or pressure of inert gas, that is, $K_i = (\partial q_i/\partial c_i)_{T,P}$.

It the gaseous mixture behaves as an ideal gas, then $c = P/R_gT$, where P is the local pressure, which remains constant in time over each switching interval of the cycle, and R_g is the ideal gas constant. Using this assumption and taking into account Eq. 5, Eq. 7 can be simplified to yield

$$(1 + \phi K_i)\frac{\partial y_i}{\partial t} = v\frac{\partial}{\partial z}\left(\frac{H_i}{2}\frac{\partial y_i}{\partial z}\right) - v\frac{\partial y_i}{\partial z} \tag{9}$$

The usual boundary conditions for Eq. 9 are

$$y_i - \frac{H_i}{2}\frac{\partial y_i}{\partial z} = y_i^{\mathrm{in}} \quad \text{for} \quad z = 0 \tag{10}$$

$$\frac{\partial y_i}{\partial z} = 0 \quad \text{for} \quad z = L \tag{11}$$

where y_i^{in} is the mole fraction of component i in the inlet gas.

For one-dimensional (I–D) flow, the interstitial fluid velocity can be expressed as[41–43]

$$v = -\frac{2(\mathrm{d}P/\mathrm{d}z)}{\alpha + \sqrt{\alpha^2 - 4\beta c|\mathrm{d}P/\mathrm{d}z|}} \tag{12}$$

where $\alpha = 150\mu(1 - \varepsilon)^2/(\varepsilon d_p)^2$ and $\beta = 1.75M_w(1 - \varepsilon)/(\varepsilon d_p)$ are the coefficients of Ergun's correlation,[44] d_p is the particle diameter, and μ and M_w are the viscosity and molecular weight of the gas, respectively. For an ideal gas Eqs. 5 and 12 can be integrated to yield the pressure and velocity profiles along the column

$$\frac{P_{\mathrm{in}}^2 - P^2}{v_{\mathrm{in}}P_{\mathrm{in}}} = 2\left(\alpha + \frac{\beta}{R_gT} v_{\mathrm{in}}P_{\mathrm{in}}\right)z, \quad v = v_{\mathrm{in}}P_{\mathrm{in}}/P \tag{13}$$

where script "in" indicates conditions at column inlet. If the pressure drop is negligible, that is, $P(z) = P_{\mathrm{in}}$, then the velocity of the flowing gas is constant throughout the column, because under dilute adsorbate conditions the mass-transfer zone is assumed to have negligible impact on the fluid velocity. It is worth noting that Eq. 9 is formally identical to the one used in HPLC, that is, under constant velocity conditions.

Materials and System Characterization

To experimentally explore the SMB process for adsorptive separation from the gas phase, the separation of the model mixture CH_4/CO_2 on activated carbon is studied. Nitrogen is used as mobile phase, acting as diluting carrier gas for the feed stream and as eluent. Based on the selectivity for the linear range of this separation problem, $K_{CO2}/K_{CH4} = 2.9$, its difficulty can be loosely classified in the easy-to-moderate range. Therefore, it is certainly not the best choice for assessing the performance and competitiveness of SMB against other cyclic adsorption processes for gas-phase separation, such as pressure-swing adsorption.[4] Separations exhibiting lower selectivity values would be more appropriate for this task. Nevertheless, the present choice is suitable for demonstrating the feasibility of the process, exploring the effect of its major operating parameters, and illustrating the performance enhancements that are obtained by using more advanced cyclic operation schemes.

The adsorbent employed in the experiments is a coal based, high-activity (109% CTC), extruded carbon (2 mm dia. pellets), courtesy from Sutcliffe Speakman Carbons Ltd (U.K.). The pore structure of the carbon was characterized by nitrogen adsorption at 77 K and mercury porosimetry. A few structural parameters for this carbon are listed in Table 1. The carbon was carefully packed into the column up to a bed height $L = 40$ cm. The amount of carbon packed into the column was 128.7 g, which is in very good agreement with the expect packing density of 0.4 g/cm^3. Research-grade nitrogen, carbon dioxide and methane, were purchased from Air Liquide, Portugal.

In the working range of gas velocity used in this work, the contribution of axial molecular diffusion is negligible, and one can consider the Péclet number Pe_i as being approximately independent of v. Furthermore, adsorption kinetics is usually governed by intraparticle diffusion rather than by external film resistance, which means that k_i is usually independent of v. Under these assumptions, the influence of v on column efficiency simplifies into a linear relationship

$$\frac{h_i}{2} = \frac{1}{\mathrm{Pe}_i} + \alpha_i v, \quad \alpha_i = \frac{\phi K_i}{k_i L(1 + \phi K_i)^2} \tag{14}$$

The Henry constants and simplified Van Deemter plots were determined by fitting the output of the chromatographic model, Eqs. 8–11, to a series of experimental chromatograms obtained by injecting diluted pulses of each adsorbate at different molar flow rates of carrier gas. The values are listed in Table 2. This is

Table 1. Adsorbent Characterization

Specific pore volume, V_p (cm^3/g)	0.86	Mean particle length, l_p (mm)	5.37
Particle porosity, ε_p	0.656	Mean particle diameter, d_p (mm)	2.15
Bulk density, ρ_b (g/cm^3)	0.40	Particle hydraulic diameter, d_p' (mm)	3.33

Table 2. Column Characterization and Adsorption Parameters

	L (cm)	d (cm)	ε	ε*
	40.0	3.2	0.476	0.820
	K	Pe	αL (s)	k (s^{-1})
CH_4	10.61	252.8	0.343	0.21
CO_2	31.10	253.7	0.377	0.07

$\varepsilon^* = \varepsilon + (1-\varepsilon)\varepsilon_p$.

equivalent to determining K_i, Pe_i and α_i from a moment analysis of the same experiments. Our procedure, however, is more general, because it can take into account peak distortion due to an axial velocity profile in the column. In practice, each pulse was approximated through the injection of a small amount of adsorbate by operating the respective mass-flow controller in a pulselike manner. In these experiments the column was operated at 36°C and four bar to reproduce the operating conditions of the separation experiments which were subsequently performed. The Henry constants obtained from the pulse tests were also checked against the equivalent values obtained from the measured stoichiometric times for a small set of breakthrough/purge experiments. The Henry constants calculated by the two methods were found to be in good agreement, as shown in Figure 3.

Cycle Definition and Optimization

We adopt a recently developed[28] compact representation of synchronous and asynchronous SMB processes as a convenient framework for defining cycle policies and optimizing operating conditions. Using this methodology one can easily derive a broad class of physically realizable asynchronous port switching schemes, univocally defined by four real parameters, $N_I,\ldots,N_{IV}$ (provided that $N = \Sigma N_j$ is an integer), which define the average zone lengths measured with respect to column length. If the N_j values are all integers, the classical SMB process with N_j columns in zone j is obtained.

To establish a particular cycle, it is sufficient to specify for one column, say column j, the time interval applicable to each clause in Eq. 1, the flow rate profile in the column, and the time intervals during which the outlet effluent of that same column is partially taken off as product. The other columns undergo the same cycle, but staggered in time by multiples of the switching interval, that is

$$\Omega_j(t) = \Omega(t_j), \quad t_j = [t-(j-1)\tau] \mod N\tau \tag{15}$$

where Ω_j denotes the set of inputs for column j, which includes Q_j, and the state (opened or closed) of its inlet/outlet ports, and "mod" defines the usual modulo operator: $a \bmod b \equiv a - b\,\mathrm{int}(a/b)$.

For convenience, the column which is selected to define the cycle for the class of asynchronous port switching schemes analyzed in this work is the last one to be regenerated, that is the last one to which its upstream effluent is admixed with fresh eluent. A more concise representation of the cycle is obtained, if the N_j's are replaced by θ_j's as defined next

$$\theta_j = \sum_{k=j}^{4} N_k, \quad j = 1,\ldots,4 \tag{16}$$

Note that each θ_j represents a cumulative zone length, and that by definition θ_1 is always equal to the total number of columns. The temporal profile of internal flow rate in the column is then defined by the following $N\tau$-periodic piecewise-constant function

$$Q(\theta) = \begin{cases} Q_{IV}, & 0 < \theta' < \theta_4 \\ Q_{III}, & \theta_4 < \theta' < \theta_3 \\ Q_{II}, & \theta_3 < \theta' < \theta_2 \\ Q_I, & \theta_2 < \theta' < \theta_1 \end{cases} \tag{17}$$

where $\theta = t/\tau$ and $\theta' = \theta \bmod N$ (the process is $N\tau$-periodic). The intervals over which the clauses in Eqs. 1 and 3 apply are listed in Table 3.

It is worth mentioning that this formulation encompasses both closed-loop ($Q_{IV} > 0$) and open-loop ($Q_{IV} = 0$) SMB schemes, as well as the typical three-zone, open-loop SMB ($N_{IV} = 0$. $Q_{IV} = 0$)[3,45,46], which can actually also operate in closed-loop ($Q_{IV} > 0$). In fact, nonnegative average zone lengths can be specified at will as long as the following con-

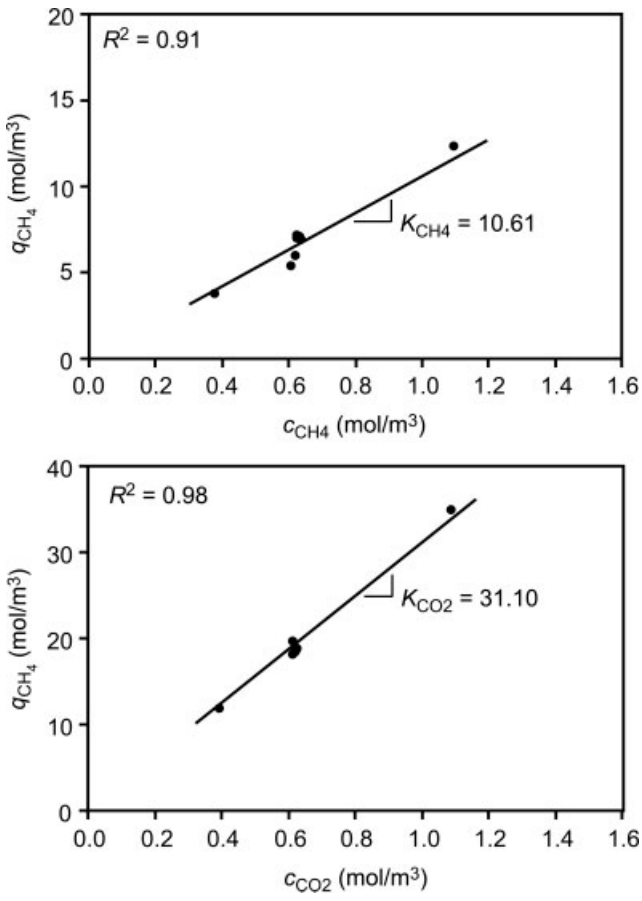

Figure 3. Adsorption isotherms on activated carbon for methane (CH_4) and carbon dioxide (CO_2) diluted in nitrogen at 36°C, total system pressure of 4 bar, and adsorbate mole fractions up to 1%.

The slope of each line represents the corresponding Henry constant obtained from pulse elution data, which were correlated with Eq. 9. The symbols represent the analysis of breakthrough/purge experiments carried out for different adsorbate mole fractions in the feed stream at 36°C and 4 bar.

Table 3. Intervals over which the Clauses in Eqs. 1 and 3 apply: $\theta_j = \Sigma_{k=j}^{4} N_k$, $\theta' = (t/\tau) \bmod N$

Eq.	Clause	Valid range
1	Feed port opened	$\theta_3 - 1 < \theta' < \theta_3$
1	Eluent port opened	$\theta_1 - 1 < \theta' < \theta_1$
3	Raffinate withdrawal	$\theta_4 < \theta' < \theta_4 + 1$
3	Extract withdrawal	$\theta_2 < \theta' < \theta_2 + 1 \quad (N_I \geq 1)$
3	Extract withdrawal	$0 < \theta' < \theta_2 + 1 - \theta_1$ and $\theta_2 < \theta' < \theta_1 \quad (N_I < 1)$

Note: This table supersedes Table 2 of Ref. 36 which was incorrectly typeset.

straints are obeyed

$$N_I + N_{II} \geq 1, \quad N_{II} + N_{III} \geq 1, \quad N_{III} + N_{IV} \geq 1, \quad N_{IV} + N_I \geq 1 \quad (18)$$

These constraints state that in order to obtain a physically realizable scheme, every two consecutive zones must span on average at least one column in length.[28]

For liquid-phase separations, the maximum allowable internal flow rate is constrained by either the capacity of the installed recycle pump, or by the efficiency and functionality of the stationary phase, which in most cases is guaranteed up to a maximum interstitial velocity, or by the maximum pressure drop in the unit. In the present case the internal flow rate is constrained by the capacity of the installed mass flow rate controllers. Because zone I exhibits the highest flow rate, the constraint on the internal flow rate can be simply expressed as $Q_I \leq Q_{max}$.

Our previously developed optimization approach[28,38] is employed here to get optimized operating conditions for the classical SMB process, in which the inlet/outlet ports are synchronously shifted, and for Varicol operation. The chosen objective function is the maximization of specific productivity Q_F/N, which for a fixed number of columns is equivalent to the maximization of feed throughput Q_F. The nonlinear programming (NLP) problem is summarized in Table 4. The NLP problem is formulated in AMPL.[47] and solved using a efficient interior-point solver,[48] as recently advocated by others.[29]

Results and Discussion

The CH_4/CO_2 separation is carried out experimentally at 36°C and four bar, which is one bar above the lowest value controlled by the installed BPR for a downstream pressure of 1 atm. The feed stream comprises a dilute mixture of 0.5% CO_2 and 0.5% CH_4 in nitrogen to place the separation in the linear

Table 4. Outline of SMB Optimization Problem

Degrees of freedom
$\tau > 0, \quad Q_I \geq 0, \ldots, Q_{IV} \geq 0, \quad N_I \geq 0, \ldots, N_{IV} \geq 0$
Objective function
$f_{obj} = \max\{Q_F\}$
Basic constraints
$Q_I \leq Q_{max}, \quad Q_{III} \leq Q_{max}, \quad \Sigma N_j = N$
Feasibility constraints on internal flowrates
$Q_{II} < Q_I, \quad Q_{III} > Q_{II}, \quad Q_{IV} < Q_{III}, \quad Q_I > Q_{IV}$ $(Q_X > 0) \quad (Q_F > 0) \quad (Q_R > 0) \quad (Q_E > 0)$
Feasibility constraints on section length
$N_I + N_{II} \geq 1, \quad N_{II} + N_{III} \geq 1, \quad N_{III} + N_{IV} \geq 1, \quad N_{IV} + N_I \geq 1$
Purity requirements
$P_R = \frac{\int Q_R y_1^R d\theta}{\int Q_R (y_1^R + y_2^R) d\theta} \geq P_R^{min}, \quad P_X = \frac{\int Q_X y_2^X d\theta}{\int Q_X (y_1^X + y_2^X) d\theta} \geq P_X^{min}$

Table 5. Operating Parameters for the 4-Column SMB Schemes Which have been Reproduced Experimentally

Run	Operating mode	τ	Q_E/Q_F	Q_F	Q_E	Q_X	Q_R	Q_{IV}
1	SMB	9.22	2.44	38.9	94.9	88.4	45.4	28.1
2	Varicol	8.02	2.10	58.6	123.0	84.7	96.9	0

Column configuration: (run 1) 1/1/1/1, (run 2) 1.38/1.06/1.56/0.
In all cases, the extract and raffinate products are 98 mol-% pure on an eluent-free basis, and the internal flow rates do not exceed 123 mmol/min. Feed throughput is maximized in both cases. Flow rates are expressed in mmol/min and τ in minutes.

adsorption range. The number of columns is fixed at four. The minimum purity for both product streams is somewhat arbitrarily fixed at 98.0 mol-% on an eluent-free basis. Given that the SMB schemes considered here do not generate any waste streams, the feedstock is fully distributed over the extract and raffinate products. Consequently, the two adsorbates are recovered at the same level as the imposed purity value because the system is fed with equal amounts of the two components. Q_{max} is fixed at 123 mmol/min. For this flow rate range, the pressure drop across the column was found to be negligible due to the large particle size of the adsorbent bed.

The first configuration analyzed is the classical 4-column SMB process, that is one column per zone, for which the feed throughput was maximized subjected to the aforementioned constraints. The optimized operating parameters are listed in the first row of Table 5. The optimized feed flow rate is $Q_F = 38.9$ mmol/min for a specific eluent consumption $Q_E/Q_F = 2.44$.

The optimized 4-column SMB process was successfully reproduced experimentally by our single-column setup, as demonstrated in Figure 4. In the topmost graph of this figure the imposed total molar flow rate, $Q(t)$, given by Eq. 17, is compared to the experimental one obtained by summing the measured values recorded by the three MFCs. Note that, because the flow rate through the MFC, which controls the admission of carrier gas is much greater than the flow rates through the other two MFCs, one has $Q_3(t) \approx Q(t)$. In order to save space the other two measured flow rates are not reproduced here, but basically the same information is conveyed in middle graph of Figure 4. This plot compares the imposed inlet composition profile, obtained from Eq. 1, with that achieved experimentally. The latter was inferred from the measured values reported by the three MFCs, that is

$$\{y_i^{in}\}^{exp} = 100 \frac{\{Q_i\}^{exp}}{\{Q_1 + Q_2 + Q_3\}^{exp}} \quad (19)$$

Again, there is good agreement between imposed and experimentally obtained profiles, though the sudden decrease of y_{CH4}^{in} at dimensionless instants $\theta = 2$, 6 and 10, is not well reproduced.

Probably the most important information conveyed by Figure 4 is provided in its bottom graph, where the experimental outlet effluent composition, $\{y_i^{out}\}^{exp}$, measured by mass spectrometry, is compared with the steady periodic solution obtained from the process model. The agreement between experimental and simulated data is excellent, which to a certain extent justifies feeding back the column with simulated data. Note that Figure 4 provides the steady periodic dynamics for a

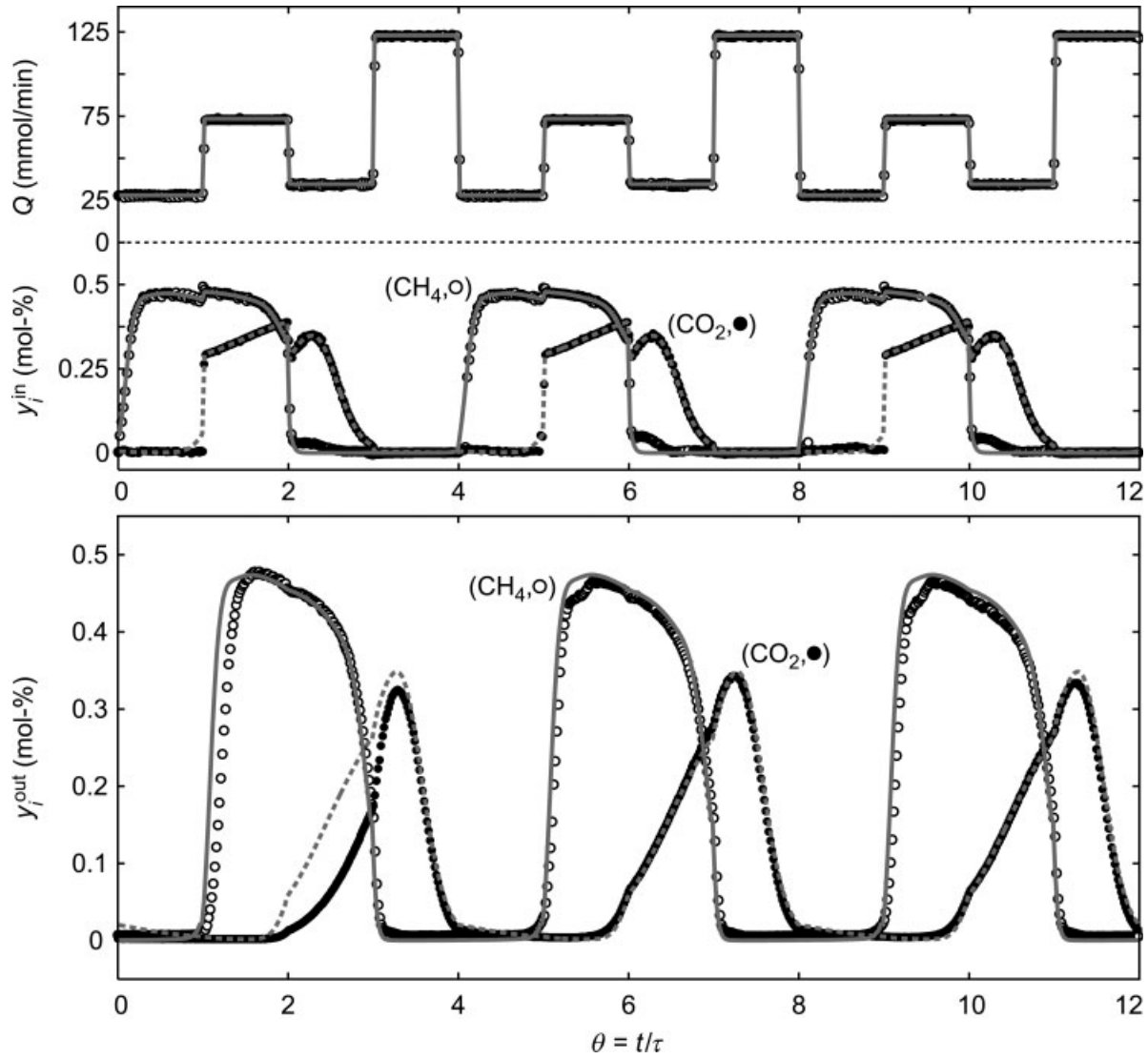

Figure 4. Experimental (symbols) and simulated (lines) temporal profiles of total molar flow rate ($Q = Q_{N2} + Q_{CH4} + Q_{CO2}$), inlet composition ($y_i^{in}$) and outlet composition (y_i^{out}), of the gas flowing through the column for the three cycles of operation of run 1 listed in Table 5.

The inlet composition is inferred from the measured values of individual molar flow rate provided by the output signals of the three mass-flow controllers placed at the column inlet, that is, $y_i^{in} = 100Q_i/Q$; the values of y_i^{out} were measured by mass spectrometry. Every cycle, fresh feed and carrier gas are added during $1 < \theta < 2$ and $3 < \theta < 4$, respectively; extract is taken off during $1 < \theta < 2$ and raffinate is withdrawn during $3 < \theta < 4$.

single column. The three nonexistent columns would have similar dynamics, but shifted in time according to Eq. 15.

Note that the column, whose behavior is reproduced experimentally, is the one whose upstream effluent is admixed with fresh carrier gas during the last switching interval of the cycle (c.f. Table 3). Hence, it is the column whose steady periodic state at the start of each cycle is closer to that of a clean column. However, this is precisely the state of the column at the startup of the experiment. Under these conditions the single-column setup should approach the cyclic steady state in a minimum number of cycles, because the initial condition for the column is the closest to its periodic state at multiples of the cycle duration (N_τ). Figure 4 shows that this is indeed the case. The second cycle is seen to have already attained the steady periodic behavior.

It should be pointed out that this procedure cannot be applied to a real SMB process because the multicolumn unit lacks the ability to artificially generate a prescribed inlet composition profile. Other authors,[49,50] however, have satisfactorily solved the problems of shortening the initial transient period, and recovering the residual adsorbates in a real SMB shutdown process.

In the second experiment reported here, the average zone lengths were added to the set of optimization variables to obtain an optimized asynchronous port switching scheme (Varicol process[15]). The optimized operating parameters for this process are listed in the second row of Table 5, and the corresponding chronogram of port switching displayed in Figure 5. Shifting the inlet/outlet ports asynchronously, in an optimal manner, is seen to enhance process performance significantly,

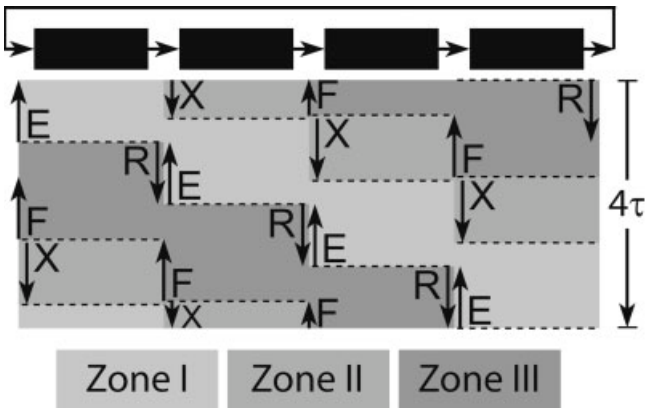

Figure 5. Chronogram of port switching for the optimized asynchronous SMB process listed as run 2 in Table 5.

Note that this scheme corresponds to a three-zone ($N_{IV} = 0$), open-loop ($Q_{IV} = 0$) SMB process.

as demonstrated by the 50.6% increase in feed throughput, and nearly 10% savings in consumption of carrier gas. Interestingly, the optimized configuration turns out to be a three-zone, open-loop SMB. This scheme does not have any recycle stream ($Q_{IV} = 0$). Furthermore, clean carrier gas is introduced into the system at the maximum allowed flow rate, $Q_E = Q_{max}$. It is reported in the literature[14] that the open-loop system has better pump stability. However, the synchronous three-zone SMB is also known to increase eluent usage and dilution of the raffinate. To a certain extent the second remark holds true for the present scheme, since the raffinate flow rate is increased from $Q_R^{(1)} = 45.4$ mmol/min to $Q_R^{(2)} = 96.9$ mmol/min, whereas the extract stream is withdrawn at about the same flow rate as for the classical closed-loop SMB scheme.

Figure 6 is similar to Figure 4, but applies to the experimentally reproduced asynchronous scheme (run 2). Again it is seen that the agreement between experimental and simulated data is excellent, and that cyclic steady state is attained within the first two cycles of operation. Thus, the simulation computer model matches the analog model (the column itself) when both models have the same cyclic steady state input. This was shown previously for liquid systems[36] and is shown in this article for gas systems. This provides further evidence that our model captures the main features of the separation process, and that it can be confidently employed for exploring other regions of the operational space.

The internal composition profile circulating around the multicolumn loop can be inferred from experimental data, such as those plotted in the bottom graphs of Figure 4 and Figure 6, as is often the case when the usual practice of sampling the concentration over the cycle at the inlet or outlet of a fixed column in the loop is adopted.[15] However, if the process model is shown to accurately reproduce the dynamics of the experimental unit, as is the case here, then the internal composition profiles are more readily obtained from the model. This is done in Figure 7, which shows the simulated axial composition profiles in gas phase, taken at half switching interval under steady periodic conditions, for the experimental runs listed in Table 5.

The optimized asynchronous scheme increases the lengths of zone I and zone III, and eliminates zone IV. The removal of this zone, which acts as buffer zone to enrich the raffinate and to recycle the carrier gas, does not affect the extract. In fact, it prevents the fast moving adsorbate from wrapping around into zone I and contaminating the extract. However, since clean carrier gas is no longer recycled back to zone I, the length of this zone must be increased in order to effectively regenerate the adsorbent. By enlarging zone III the system can withstand more heavily loaded columns, that is, the axial composition profiles are increased to higher concentrations. This results in a considerable gain in productivity without incurring in an undesirable increase of eluent consumption.

Figure 8 compares the Pareto optimal solutions for synchronous and asynchronous SMB operations. Each curve represents the opposing objectives of increasing productivity and decreasing eluent consumption for a given scheme, whose conflict can only be resolved if other considerations, such as the overall separation cost, are taken into account. In all of the optimization runs, the purity constraints are always active. The open circles locate the two experimental runs reported in Table 5. Under both experimental conditions the constraint on the maximum allowable internal flow rate is also active; this condition must be dropped in order to extend the Pareto curves past the open circles towards higher feed flow rates.

Note that Figure 8 shows the full extent of the Pareto curve for synchronous SMB operation, but displays only the lower portion of the Pareto curve for asynchronous port switching. The latter extends the attainable productivities well above those reached by the classical SMB process. As can be seen in the figure, the asynchronous operating scheme outperforms the standard SMB operating scheme, both in productivity and eluent consumption, because of the increased degrees of freedom. This is especially true in the higher feed throughput region. It is also interesting that the optimal values of both schemes collapse into a single curve in the low-range of feed flow rate. In fact, for Q_F values below $\approx$ 30 mmol/min, the optimized average zone lengths approach those of the classical SMB scheme as the feed flow rate is decreased.

Our class of optimized Varicol processes, which are defined by Eq. 17 and Table 3, is to a large extent the discrete analog of the equivalent true moving-bed process with optimized zone lengths. This is achieved by modulating over a switching interval the number of columns in each section, so that on average the optimized column configuration 1.38/1.06/1.56/0 is obtained.

It is clear that a conventional four-column SMB process has little flexibility with respect to zone length manipulation. Besides the 1/1/1/1 configuration, the only feasible options are moving the column from zone II or zone IV to another zone. However, a classical N-column SMB process can approximate any noninteger zone length, say N_j, by the nearest integer number of columns, int($N_j + 0.5$), with a relative error which is at most equal to $0.5/N$. This approximation improves with increasing number of columns. It is thus clear that the superiority of the Varicol process over a conventional SMB process decreases with increasing number of columns, because the desired zone lengths can be equally achieved without the need to modulate the column configuration.

For a linear separation, the thermodynamic limit for the specific eluent consumption without adding energy to the system is $Q_E/Q_F = 1$.[51] This value can be compared to the limiting value, $Q_E/Q_F \approx 1.25$, attained by both Pareto curves as Q_F

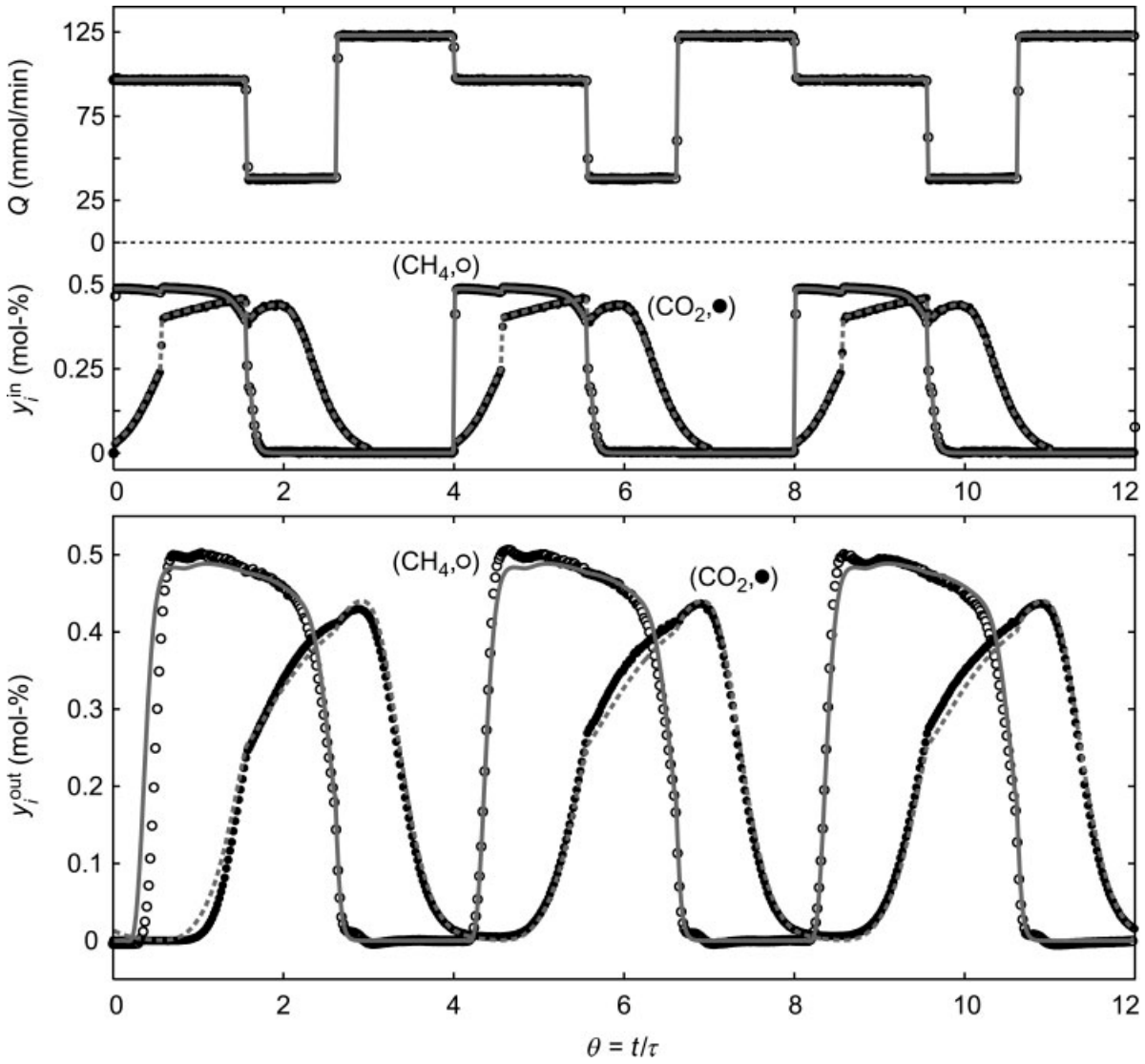

Figure 6. Same profile information as plotted in Figure 4, but for run 2 of Table 5.

The dimensionless periods during which fresh feed and eluent are added, and extract and raffinate are withdrawn, are respectively, [0.56, 1.56], [3, 4], [0, 1] and [2.62, 3.62].

approaches zero. One should be cautious, however, when comparing the performance of a real system against the thermodynamic limit, because the latter is obtained from an equilibrium analysis of the true moving-bed model, which neglects finite mass-transfer resistances and assumes an infinite number of differential columns.

Conclusions

In this work, we have investigated gas separation by SMB using a weakly circulating desorbent, which acts as carrier gas for the components being separated and regenerates the adsorbent by eluting the mixture. The experimental feasibility and effectiveness of this process were assessed by running and comparing optimized configurations for the separation of CH_4/CO_2 over activated carbon using nitrogen as carrier gas.

A novel single-column experimental setup was employed to demonstrate the feasibility of the process, explore the effect of its major operating parameters, and illustrate the performance enhancements that are obtained by using an advanced cyclic operation scheme, such as the asynchronous shifting of the inlet/outlet ports. The simulated outlet effluent composition was in excellent agreement with the measured one for the two experimental runs reported here. This is expected since the adsorption equilibrium is simple, band broadening is well taken into account, and the inherent experimental variabilities derived from multicolumn packing are absent in our setup. It was also shown that by correctly selecting the step of the cycle for process startup, the steady periodic behavior is reproduced in a very short experimental run (1–3 cycles) with minimal consumptions of gaseous eluent and adsorbates.

For the separation under study, the asynchronous configuration always outperforms the classical SMB scheme, both in productivity and eluent consumption, except for very low-feed throughputs where both schemes are coincident. At higher feed

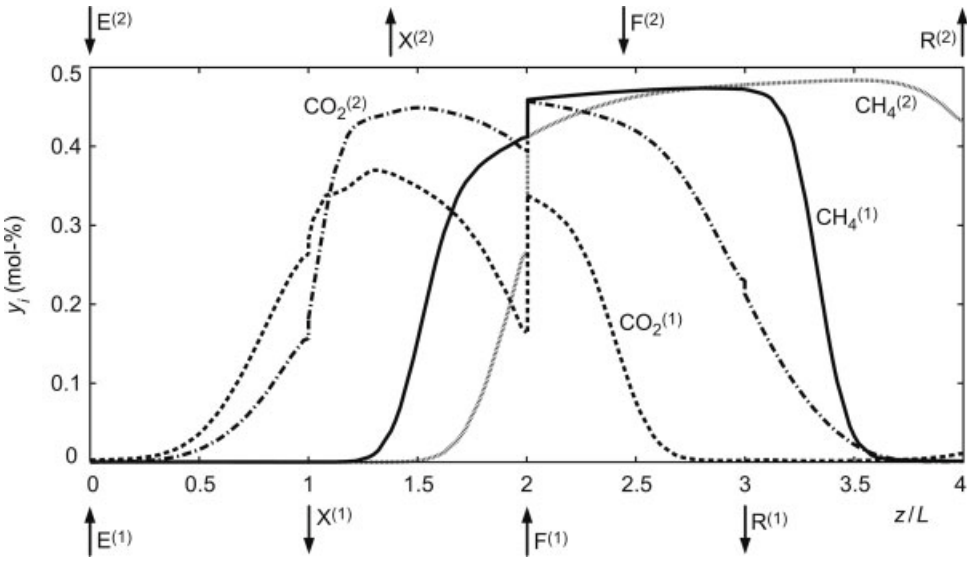

Figure 7. Simulated axial composition profiles in gas phase, taken at half switching interval under steady periodic conditions, for the two runs listed in Table 5.

flow rates, the asynchronous scheme quickly diverges from a four-zone, closed-loop configuration towards a three-zone, open-loop process.

The work is currently being extended to the nonlinear region of the adsorption equilibrium, where the process operates under nonisothermal conditions with nonnegligible changes in fluid velocity across the mass-transfer zone. The use of pressure swing to induce both desorption and flow of gas through the columns is also being evaluated.

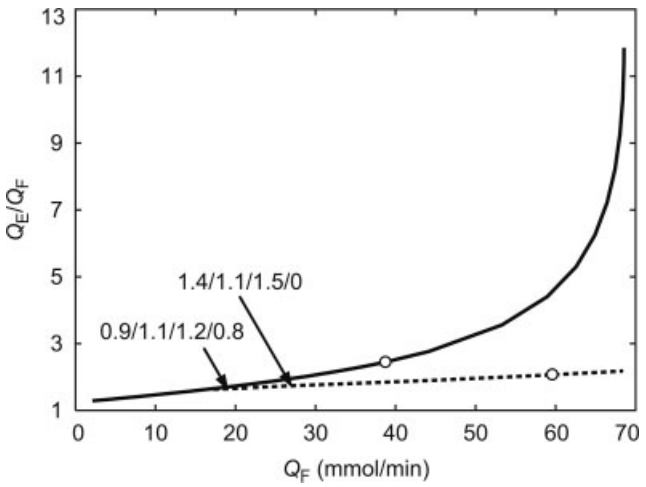

Figure 8. Pareto-optimal solutions for synchronous (solid line) and asynchronous (dashed line) port switching schemes.

The Pareto curve for synchronous operation is plotted in its entirety but that for asynchronous port switching is only partially plotted and extends to the right of the x-axis. The open circles locate the two experimental runs listed in Table 5. Note that the constraint on the maximum admissible internal flowrates was relaxed in order to obtain the part of the curve to the right of each circle.

Acknowledgments

Support from FCT/MCES (Portugal), through project POCTI/EQU/39391/2001 and Postdoctoral grant SFRH/BPD/14910/2004, is gratefully acknowledged.

Notation

c = gas concentration, mol/cm^3
D_L = axial dispersion coefficient, cm^2/min
h = dimensionless plate height
k = LDF coefficient, min^{-1}
K = Henry's constant
L = column length, cm
N = number of columns
Pe = Péclet number
q = adsorbed concentration, mol/cm^3
Q = molar flow rate, mol/min
t = time, min
v = interstitial gas velocity, cm/min
y = mole fraction
z = axial position in column, cm

Greek letters

ϕ = phase ratio, $(1-\varepsilon)/\varepsilon$
ε = interparticle porosity
ε^* = total bed porosity
ε_p = particle porosity
τ = switching interval, min
θ = dimensionless time, t/τ

Subscripts and superscripts

E = eluent
exp = experimental
F = feed
i = adsorbate index
I,...,IV = zone index
in = inlet effluent
j = column index
out = outlet effluent
R = raffinate
sim = simulated
X = extract

Literature Cited

1. Storti G, Mazzotti M, Morbidelli M, Carrà A. Robust design of binary countercurrent adsorption separation processes. *AIChE J*. 1993;39:471.
2. Mazzotti M, Storti G, Morbidelli M. Optimal operation of simulated moving bed units for nonlinear chromatographic separations. *J Chromatogr A*. 1997;769:3.
3. Ruthven DM, Ching CB. Countercurrent and simulated countercurrent adsorption separation processes. *Chem Eng Sci*. 1989;44:1011.
4. Yang RT. Gas separation by adsorption processes. London: Imperial College Press. 1997.
5. Storti G, Mazzotti M, Furlan LT, Morbidelli M, Carrà S. Performance of a six port simulated moving bed pilot plant for vapor-phase adsorption separations. *Sep Sci Technol*. 1992;27:1889.
6. Mazzotti M, Baciocchi R, Storti G, Morbidelli M. Vapor-phase SMB adsorptive separation of linear/nonlinear paraffins. *Ind Eng Chem Res*. 1996;35:2313.
7. Juza M, Di Giovanni O, Biressi G, Schurig V, Mazzotti M, Morbidelli M. Continuous enantiomer separation of the volatile inhalation anesthetic enflurane with a gas chromatographic simulated moving bed unit. *J Chromatogr A*. 1998;813:333.
8. Biressi G, Quattrini F, Juza M, Mazzotti M, Schurig V, Morbidelli, M. Gas chromatographic simulated moving bed separation of the enantiomers of the inhalation anesthetic enflurane. *Chem Eng Sci*. 2000;55:4537.
9. Biressi G, Mazzotti M, Morbidelli M. Experimental investigation of the behavior of gas phase simulated moving beds. *J Chromatogr A*. 2002;957:211.
10. Biressi, G, Rajendran, A, Mazzotti, M, Morbidelli, M. The GC-SMB separation of the enantiomers of isoflurane. *Sep Sci Technol*. 2002;37:2529.
11. Rothchild RD. Gas separation by continuous pressure-swing chromatography. US Pat. 5,672,197; 1997.
12. Abe T, Tanzawa S, Masuda T. Method and apparatus for separating, removing, and recovering gas components. US Pat. 6,461,410 B1; 2002.
13. Cheng LS, Wilson ST. Process for separating propylene from propane. US Pat. 6,293,999 B1; 2001.
14. Chin CY, Wang NHL. Simulated moving bed equipment designs. *Sep Purif Rev*. 2004;33:77.
15. Ludemann-Hombourger O, Nicoud RM, Bailly M. The Varicol process: a new multicolumn continuous chromatographic process. *Sep Sci Technol*. 2000;35:1829.
16. Ludemann-Hombourger O, Pigorini G, Nicoud RM, Ross DS, Terfloth G. Application of the Varicol process to the separation of the isomers of the SB-553261 racemate. *J Chromatogr A*. 2002;947:59.
17. Kearney MM, Hieb KL, Time variable simulated moving bed process. US Patent 5,102,553; 1992.
18. Kloppenburg E, Gilles ED. A new concept for operating simulated moving-bed process. *Chem Eng Technol*. 1999;22:313.
19. Zang Y, Wankat PC. SMB operation strategy: partial feed. *Ind Eng Chem Res*. 2002;41:2504.
20. Zhang Z, Mazzotti M, Morbidelli M. PowerFeed operation of SMB units: changing the fluid flow rates during the switching interval *J Chromatogr A*. 2003;1006:87.
21. Zhang Z, Mazzotti M, Morbidelli M. Experimental assessment of PowerFeed chromatography *AIChE J*. 2004;50:625.
22. Schramm H, Kaspereit M, Kienle A, Seidel-Morgenstern A. Improving simulated moving bed process by cyclic modulation of the feed concentration. *Chem Eng Technol*. 2002;25:1151.
23. Schramm H, Kaspereit M, Kienle A, Seidel-Morgenstern A. Simulated moving bed process with cyclic modulation of the feed concentration. *J Chromatogr A*. 2003;1006:77.
24. Dünnebier G, Klatt KU. Optimal operation of simulated moving bed chromatographic processes. *Comput Chem Eng*. 1999;23:S189.
25. Jupke A, Epping A, Schmidt-Traub H. Optimal design of batch and simulated moving bed chromatographic separation processes. *J Chromatogr A*. 2002;944:93.
26. Toumi A, Hanisch F, Engell S. Optimal operation of continuous chromatographic processes: mathematical optimization of the VARICOL process. *Ind Eng Chem Res*. 2002;41:4328.
27. Toumi A, Engell S, Ludemann-Hombourger O, Nicoud RM, Bailly M. Optimization of simulated moving bed and varicol processes. *J Chromatogr A*. 2003;1006:15.
28. Araŕjo JMM, Rodrigues RCR, Mota JPB. Optimal design and operation of a certain class of asynchronous simulated moving bed processes. *J Chromatogr A*. 2006;1132:76.
29. Kawajiri Y, Biegler LT. Optimization strategies for simulated moving bed and Power Feed processes. *AIChE J*. 2006;52:1343.
30. Kawajiri Y, Biegler LT. Nonlinear programming superstructure for optimal dynamic operations of simulated moving bed processes. *Ind Eng Chem Res*. 2006;45:8503.
31. Kloppenburg E, Gilles ED. Automatic control of the simulated moving bed process for C_8 aromatics separation using asymptotically exact input/output linearization. *J Process Control*. 1999;9:41.
32. Klatt KU, Hanisch F, Dünnebier G, Engell S. Model-based optimization and control of chromatographic processes. *Comput Chem Eng*. 2000;24:1119.
33. Klatt KU, Hanisch F, Dünnebier G. Model-based control of a simulated moving bed chromatographic process for the separation of fructose and lactose. *J Process Control*. 2002;12:203.
34. Schramm H, Grüner S, Kienle A. Optimal operation of simulated moving bed chromatographic processes by means of simple feedback control. *J Chromatogr A*. 2003;1006:3.
35. Abel S, Erdem G, Amanullah M, Morari M, Mazzotti M, Morbidelli M. Optimizing control of simulated moving bed—experimental implementation. *J Chromatogr A*. 2005;1092:2.
36. Rodrigues RCR, Araújo JMM, Eusébio MFJ, Mota JPB. Experimental assessment of simulated moving bed and varicol processes using a single-column setup. *J Chromatogr A*. 2006; doi:10.1016/j.chroma.2006.10.044.
37. Mota JPB, Araújo JMM. Single-column simulated moving-bed with recycle lag. *AIChE J*. 2005;51:1641.
38. Araújo JMM, Rodrigues RCR, Mota JPB. Use of single-column models for efficient computation of the periodic state of a simulated moving-bed process. *Ind Eng Chem Res*. 2006;45:5314.
39. Eusébio MFJ. Development of an Universal Interface for Monitoring and Control of Chemical and Biochemical Processes Universidade Nova de Lisboa: Lisbo, Portugal; 2006. Ph.D. Thesis (in Portuguese).
40. Guiochon G, Golshan-Shirazi S, Katti A. Fundamentals of Preparative and Nonlinear Chromatography. Boston: Academic Press; 1994.
41. Mota JPB, Saatdjian E, Tondeur D, Rodrigues AE. A simulation model of a high-capacity methane adsorptive storage system. *Adsorption*. 1995;1:17.
42. Mota JPB, Rodrigues AE, Saatdjian E, Tondeur D. Charge dynamics of a methane adsorption storage System: intraparticle diffusional effects. *Adsorption*. 1997;3:117.
43. Mota JPB, Rodrigues AE, Saatdjian E, Tondeur D. Dynamics of natural gas adsorption storage systems employing activated carbon. *Carbon*. 1997;35:1259.
44. Ergun S. Fluid flow through packed column. *Chem Eng Prog*. 1952;48:89.
45. Meissner JP, Carta G. Continuous regioselective enzymatic esterification in a simulated moving bed reactor. *Ind Eng Chem Res*. 2002;41:4722.
46. Zang Y, Wankat PC. Three-zone simulated moving bed with partial feed and selective withdrawal. *Ind Eng Chem Res*. 2002;41:5283.
47. Fourer R, Gay DM, Kernighan BW. *AMPL a modeling language for mathematical programming*. 2nd ed. Pacific Grove, CA: Brooks/Cole—Thomson Learning; 2003.
48. Wächter A, Biegler LT. On the implementation of an interior point filter line search algorithm for large-scale nonlinear programming. *Math Prog*. 2005;106:25.
49. Xie Y, Mun SY, Wang NHL. Startup and shutdown strategies of simulated moving bed for insulin purification. *Ind Eng Chem Res*. 2003;42:1414.
50. Abunasser N, Wankat PC. One-column chromatograph with recycle analogous to simulated moving bed adsorbers: analysis and applications. *Ind Eng Chem Res*. 2004;43:5291.
51. Wankat PC. Large-scale adsorption and chromatography. Boca Raton, FL: CRC Press; 1986.

Manuscript received Nov. 10, 2006, and revision received Jan. 24, 2007.